Dynamical properties of copper halides. I. Interionic forces, charges, and phonon dispersion curves

G. Kanellis,* W. Kress, and H. Bilz
Max-Planck-Institut für Festkörperforschung, Heisenbergstrasse 1, D-7000 Stuttgart 80, Federal Republic of Germany
(Received 11 November 1985)

In the three papers in this series the anomalous dynamical properties of copper halides are analyzed. The present paper focuses on the interionic forces and phonons in these materials. It is shown that the partially ionic nature of these tetrahedrally coordinated semiconductors is best described by various valence-shell models which combine a valence-force-field approach with that of dipolar models (i.e., effective charge, polarizabilities, etc.). The trends of the interionic forces in the sequence CuCl→CuBr→CuI reflect the changes in the electronic band structure and the increasing tendency to superionic conductivity.

I. INTRODUCTION

The copper halides CuCl, CuBr, and CuI are borderline cases between ionic and covalent compounds.[1] They exhibit many unusual physical properties and, therefore, have attracted in recent years considerable experimental and theoretical interest.

As do most of the covalent III-V and II-VI compounds, the copper halides crystallize in the tetrahedrally coordinated zinc-blende structure. They undergo, however, at room temperature under moderate hydrostatic pressure, phase transitions into the wurtzite structure and show at high temperatures other different phases.[2–4] They have closed-shell electronic configurations with static ionic charges of about the Cu^+-ion "valency" similar to the alkali halides. The closed $3d^{10}$ shell of the Cu^+ ion plays an important role for the lattice dynamics of copper halides.

Copper halides are strongly anharmonic compounds. Their x-ray[2,5–8] and neutron[9,10] diffraction data reveal large mean-square vibrational amplitudes. At elevated temperatures they even become superionic conductors.[11,12]

The most interesting feature of the copper halides, which has attracted constant interest in recent years,[13–26] is the unusual double-peak structure of the transverse optic (TO) phonon of CuCl at the zone center (Γ). This structure has been observed in the first-order Raman spectra[13–25] as well as in the inelastic neutron scattering spectra.[26] The latter show that the anomalous line shape is not restricted to Γ-point phonons. It is strongly $\mathbf{q}$ dependent and has been observed for small $\mathbf{q}$ vectors around the Γ point.

In CuBr the anomalous structure of the TO(Γ) phonon is less pronounced but still visible, especially under low hydrostatic pressure.[22] The Raman spectra of CuI exhibit a broadened TO(Γ) peak which is strongly temperature dependent.[27]

The organization of our work is as follows: In the present paper (henceforth denoted as I) we give a systematic and detailed investigation of the force constants and the phonon dispersion curves of copper halides. This analysis will serve as a basis for the second paper (II),[28] where we focus on the TO(Γ) phonon anomalies in CuCl and CuBr. It will be shown that these anomalies may be quantitatively understood in terms of Fermi resonances between the TO(Γ) phonons and two-phonon combination bands. In a third paper (III),[29] the pressure dependence of the optic phonons is investigated and changes of line shapes are calculated. Altogether, the three papers should serve as a unifying new representation of the normal and the anomalous dynamical properties of Cu halides.

II. INTERIONIC FORCES AND PHONONS

The interionic forces of the copper halides exhibit a complex behavior due to the mixture of covalent and ionic bonding. Anharmonic and nonlinear effects are to be expected.

The phonon dispersion curves of CuCl, CuBr, and CuI have been determined at room temperature from inelastic neutron scattering measurements.[30–32] These measurements have been later repeated for CuCl (Ref. 33) and CuBr (Ref. 34) at 4.2 and 77 K, respectively. In view of the strong anharmonicity of all three compounds, the determination of quasiharmonic frequencies at room temperature and, in particular, the determination of the high-frequency optic modes, is very open to discussion for both experimental and theoretical reasons. The low- and high-temperature data for CuCl are, in fact, in partial contradiction. These discrepancies are probably due to the poor sample quality and the unfavorable experimental conditions for the earlier room-temperature measurements. We, therefore, cannot rely on model calculations[35–38] which fit the room-temperature data of CuCl and so we base our analysis on the more precise data at 4.2 K. The 77-K data of CuBr (Ref. 34) reveal a crossing of the TO and LO branches in the Δ direction close to the X point, which seems to be a rather general feature of zinc blende compounds with nearly equal anion and cation masses. The room-temperature data,[31] which are less complete than the low-temperature data, do not exhibit

such a crossing. Here again we base our analysis on the low-temperature data and do not rely on model calculations[38–40] which do not reproduce this crossing. For CuI only are room-temperature data[32] available, which can be reproduced by various models.[36–38] We would like to mention two attempts to reproduce the phonon dispersion curves of all three copper halides with a unique model. The first one[41] is based on a general expression for the total energy, which includes dipolar and quadrupolar terms and gives a good overall description of different lattice mechanical properties. Unfortunately, this model does not reproduce the measured dispersion curves well enough to serve as a basis for the investigation of dynamical properties such as the line shapes. The second model is an 11-parameter rigid-ion model,[42] which gives a good overall fit to the low-temperature dispersion curves and has also been used rather successfully to reproduce the measured dispersion curves of III-V and II-VI compounds[43,44] with zinc-blende structure. The rigid-ion model has the drawback that it cannot give a description of the electronic polarizability, which plays an important role in the zinc-blende compounds. Moreover, an anharmonic extension of this model involves a large number of anharmonic parameters. By far the best model which has been proposed up to now for a systematic description of the phonon dispersion curves in III-V and II-VI compounds with the zinc-blende structure is the valence overlap shell model (VOSM).[45,46] It provides not only a good description of the measured phonon dispersion curves but gives also the correct eigenvectors for the shell displacements, which have been checked in calculating the cross sections of second-order Raman scattering using a local theory of the electronic polarizabilities.

III. THEORETICAL BACKGROUND

The shell model (SM) (Ref. 47) takes into account the displacement-induced electronic polarizabilities in the dipole approximation. It has been widely used and discussed in the literature.[48,49] Therefore we will not go into the details here.

To summarize briefly for later convenience, we write the equations of motion for cores and relative displacements of the shells in the harmonic and adiabatic approximations as

$$\begin{aligned} \underline{M}\omega^2\mathbf{u} &= (\underline{R}+\underline{Z}\,\underline{C}\,\underline{Z})\mathbf{u}+(\underline{T}+\underline{Z}\,\underline{C}\,\underline{Y})\mathbf{w}\ , \\ 0 &= (\underline{T}^{\dagger}+\underline{Y}\,\underline{C}\,\underline{Z})\mathbf{u}+(\underline{S}+\underline{K}+\underline{Y}\,\underline{C}\,\underline{Y})\mathbf{w}\ , \end{aligned} \tag{1}$$

where $\underline{M}$, $\underline{Z}$, and $\underline{Y}$ are diagonal matrices for the masses, the ionic charges and the shell charges, respectively, $\underline{C}$ accounts for the long-range Coulomb interactions and $\underline{R}$, $\underline{T}$, and $\underline{S}$ describe the short-range core-core, core-shell, and shell-shell interactions, respectively. The core-shell and shell-shell interactions are already transformed to the relative displacements of the shells $\mathbf{w}=\mathbf{s}-\mathbf{u}$, where $\mathbf{u}$ and $\mathbf{s}$ are the displacement vectors of the cores and shells, respectively. $\underline{K}$ is the diagonal matrix which describes the on-site core-shell interactions.

The general description of the short-range interactions up to second-nearest neighbors requires in the zinc-blende structure 30 parameters which specify the interaction matrices $\underline{R}$, $\underline{T}$, and $\underline{S}$. The matrix $\underline{K}$ contains the parameters k_1 and k_2, $\underline{Y}$ contains the shell charges Y_1 and Y_2, and the matrix of the ionic charges contains the parameters Z_1 and Z_2. The charge neutrality requires $Z_1=-Z_2$. The indices 1 and 2 refer to cations and anions, respectively.

We assume that the short-range forces between first- and second-nearest neighbors act only through the shells ($\underline{R}=\underline{S}=\underline{T}$). This assumption reduces the disposable short-range parameters from thirty to ten. We describe the short-range interactions in terms of valence-field coordinates to take into account the partially covalent character of these interactions in an appropriate way and to reduce further the number of general tensorial coupling constants permitted by the zinc-blende symmetry.

We assume that the potential function for the short-range (SR) interactions has the form

$$\begin{aligned} \phi^{\mathrm{SR}} = {} & \frac{\lambda}{2}\sum_{1\text{-}2}(\Delta r_{ij})^2+\frac{k_{r_1\theta}}{2}r_1\sum_{2\text{-}1\text{-}2}(\Delta\theta_{ijl})(\Delta r_{ij}) \\ & +\frac{k'_{r_1\theta}}{2}r_1\sum_{1\text{-}2\text{-}1}(\Delta\theta_{jlk})(\Delta r_{jl})+\frac{k_{r_2\theta}}{2}r_2\sum_{2\text{-}1\text{-}2}(\Delta\theta_{ijl})(\Delta r_{il}) \\ & +\frac{k'_{r_2\theta}}{2}r_2\sum_{1\text{-}2\text{-}1}(\Delta\theta_{jlk})(\Delta r_{jk})\ , \end{aligned} \tag{2}$$

where Δr_{ij} are the changes in distances between the ion i and j and $\Delta\theta_{ijl}$ are the changes in bond angles between nearest neighbors. The summation runs over all combinations 1-2, 2-1-2, and 1-2-1 for which the ions 1 and 2 are nearest neighbors and form nearest-neighbor bond angles. Equation (2) contains five short-range force constants. Thus the model has altogether ten adjustable parameters, including the charges and the on-site core-shell interactions.

Figure 1 shows schematically the different terms taken into account in the valence-force-field potential. It should be pointed out that our choice of the valence-force-field constant is different from that currently used in the literature. We replace the quadratic terms in the change of the bond angle $k_{\theta\theta}$ by a mixed term in the bond angle and second-nearest-neighbor distance change $k_{r_2\theta}$. The expansion coefficients $k_{r_1\theta}$ and $k_{r_2\theta}$ constitute a better decomposition than the use of $k_{r_1\theta}$ and $k_{\theta\theta}$, since the $k_{\theta\theta}$ terms absorb contributions from both types of angular deformations shown in Fig. 1. Moreover, the $k_{r_2\theta}$ term leads to a traceless nearest-neighbor interaction matrix

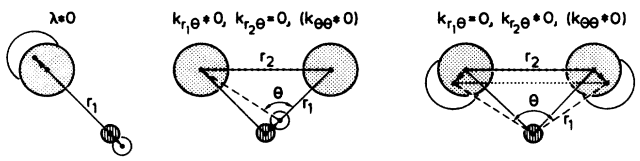

FIG. 1. Schematic representation of the valence-force-field coupling constants.

$$\phi_{\alpha\alpha}(1,2)=0\ ,$$
$$\phi_{\alpha\beta}(1,2)=\frac{4\sqrt{2}}{3}(k_{r_2\theta}+k'_{r_2\theta})\ , \tag{3}$$

which is well suited to account for quadrupolar effects. The positions of the ions 1 and 2 are (0,0,0) and $\frac{1}{4}(1,1,1)$, respectively. The coupling constants $k_{r_2\theta}$ and $k'_{r_2\theta}$ refer to angles at the cation and anion site, respectively.

The contribution to the second-nearest-neighbor interactions are

$$\phi_{xb}(1,1)=\phi_{yb}(1,1)=-\frac{\sqrt{2}}{3}k'_{r_2\theta}\ ,$$
$$\phi_{zz}(1,1)=0\ , \tag{4}$$
$$\phi_{zx}(1,1)=\phi_{zy}(1,1)=\frac{\sqrt{2}}{3}k'_{r_2\theta}\ ,$$

where the first of the ions 1 is at the position (0,0,0) and the other at $\frac{1}{2}(1,1,0)$. The expressions for the anion-anion interactions are analogous. The analytic expression for the contribution of the other valence-force-field constants to the short-range-interaction matrix $\underline{R}$ are explicitly given by Kunc and Nielson.[50]

The valence-force-field potential function ϕ^{SR} accounts for interactions due to the radial overlap of the wave functions of nearest neighbors as well as for the angular distortions of the bond angles by excitations of the hybridized states which form the directional bonds. It also takes partially into account multipolar deformations, polarization effects due to overlap between the first- and second-nearest-neighbor charge densities, exchange charge contributions, and electric multipole interactions, which decrease rapidly with increasing distance.

The extent to which this valence-force-field description is adequate depends strongly on the compound under consideration. Up to now there is no systematic investigation on a microscopic basis of the approximate form of the valence-force fields for different compounds.

Although the shell model allows for electronic polarizabilities of the ions in the dipolar approximation, it turns out that best fits to the measured phonon dispersion curves quite often yield values of the electronic polarizabilities which are smaller than those determined from the high-frequency dielectric constant ϵ_∞. The reason is that contributions from higher-order terms in the deformations of the electronic charge density may also be important and that the deformations of the real charge densities cannot always be approximated by a single displacement-induced dipole at each ion site. It also turns out that the effects of the charge-density deformations are quite often partly contained in the short-range force constants. Thus for diamond, silicon, and germanium good descriptions of the phonon dispersion curves are obtained with valence-force-field models,[51,52] which do not at all allow explicitly for displacement-induced electronic dipolar moments. Adequate descriptions of the phonon dispersion curves are even obtained with rigid-ion models, provided that the short-range interactions can absorb the effects of dipolar and multipolar polarizabilities. This can always be achieved, since the Taylor expansion of the potential in the displacements of the particles is complete, whereas the expansion in core and shell displacements is overcomplete. The advantage of the shell model is the clear and physical separation of the dipolar interactions. Moreover, the anharmonic extension of the shell model[53,54] gives the correct second-order Raman scattering cross sections and explains in a natural way the strong temperature dependence of the soft modes in ferroelectric compounds.[55,56]

An even better description of the real charge distribution and hence a better separation of the true overlap interaction can be achieved by assigning either form factors to the shells of the ions or by incorporating the higher-order terms in the multipole expansion in the model.[57,58] An alternative step beyond the dipolar approximation is the introduction of two shells at the ion sites.

Such a double-shell model[59] with two shells at the metal site has been used to describe the lattice dynamics of transition-metal carbides and nitrides. This model describes the phonon anomalies which arise from strong electron-phonon interactions at certain points of the Brillouin zone. The second shell which is coupled to the first one by an isotropic force constant reflects the interactions of the d electrons in the metal sublattice.

We adopt here a slightly different point of view. In cases where the second-nearest-neighbor correlations are strong the charge density of an ion can be represented by two shells coupled to the same core. In this model, the interactions between first-nearest neighbors are due to an overlap of charge density which is represented by the first shell. The correlations between second-nearest neighbors act through a second shell. In principle, both shells carry different charges. It is reasonable to assume that the core-shell constants of both shells are equal, since the effective restoring force constants are the sum of the on-site force constants and the coupling constants to the neighboring shells, which are adjustable parameters. Since both shells describe on-site dipoles, no interaction between two shells of the same ion is assumed. This is in contrast to the double-shell model of Weber[59] in which the second shell is coupled to the first one (inner and outer shell). It should be mentioned that a double-shell model with two on-site dipoles allows for quadrupolar deformations to be taken into account in a first approximation.

Using the same notation as in Eq. (1) the equations of motion for the double-shell model read in the adiabatic and harmonic approximation as

$$\begin{aligned}
\underline{M}\omega^2\mathbf{u}&=(\underline{\tilde{R}}+\underline{Z}\,\underline{C}\,\underline{Z})\mathbf{u}+(\underline{T}+\underline{Z}\,\underline{C}\,\underline{Y})\mathbf{w}+(\underline{T}'+\underline{Z}\,\underline{C}\,\underline{Y}')\mathbf{w}'\ ,\\
0&=(\underline{T}^{\dagger}+\underline{Y}\,\underline{C}\,\underline{Z})\mathbf{u}+(\underline{S}+\underline{K}+\underline{Y}\,\underline{C}\,\underline{Y})\mathbf{w}+(\underline{Y}\,\underline{C}\,\underline{Y}')\mathbf{w}'\ ,\\
0&=[(\underline{T}')^{\dagger}+\underline{Y}'\,\underline{C}\,\underline{Z}]\mathbf{u}+(\underline{Y}'\,\underline{C}\,\underline{Y})\mathbf{w}+(\underline{S}'+\underline{K}'+\underline{Y}'\,\underline{C}\,\underline{Y}')\mathbf{w}'\ ,
\end{aligned} \tag{5}$$

where $\underline{\tilde{R}}=\underline{R}+\underline{R}'$, $\underline{R}$, $\underline{T}$, and $\underline{S}$ are the matrices for the nearest-neighbor interactions, $\underline{R}'$, $\underline{T}'$, and $\underline{S}'$ are the second-nearest-neighbor interaction matrices, and $\underline{Y},\underline{Y}'$ and $\underline{K},\underline{K}'$ are the diagonal matrices of the charges and the on-site core-shell interactions for the first and second shell, respectively. The displacement vectors for the relative displacements of the first and second shell are $\mathbf{w}$ and $\mathbf{w}'$, respectively. The short-range interactions are calcu-

lated in the framework of the valence-force-field model and contain five adjustable parameters. Together with the parameters for the ionic charge, the shell charges and the on-site core-shell interactions, which are assumed to be the same for the first and second shell, this gives altogether 12 adjustable parameters. The discussion in the following section will show that the number of parameters can be reduced still further.

A model with two shells at the Cu^+ site has been used by Vardeny *et al.*[37] to fit the room-temperature data of CuCl.[30] These data are in partial contradiction with the more reliable low-temperature data on which our calculations are based.

IV. RESULTS AND DISCUSSION

We determine the parameters for various versions of single- and double-shell models by least-squares fits to the measured phonon dispersion curves. For CuCl and CuBr we use the low-temperature data. The fits for CuI are based on the room-temperature data, since low-temperature data are not available at present. The fitting procedure consists of minimizing the least-squares deviation

$$\chi^2=\frac{1}{N}\sum_{i=1}^{N}(\omega_{i,\mathrm{exp}}-\omega_{i,\mathrm{calc}})^2 , \tag{6}$$

where the sum over i runs over all measured phonon frequencies ω_{exp}. The parameters and the least-squares deviations obtained for different models are displayed in Table I. The various models are labeled as follows: VOSM is the valence-overlap-shell model, VSM the valence-shell model, and DSM the valence-double-shell model.

We start our discussion with the valence-overlap-shell model. This model is characterized by the positive shell charge of the Cu^+ ion which describes the overlap polarization. The ionic radius of the halogen ions increases monotonically in the series CuCl, CuBr, CuI. The repulsive force constant λ which arises from the radial overlap of the cation and anion wave functions follows this trend. The next important parameter is $k_{r_1\theta}$ on the Cu^+ site, which shows the same tendency as λ. The remaining valence-force-field parameters are rather small and do not show clear trends. The ionic charge Z remains rather constant, indicating that the increasing overlap does not result in an appreciable charge transfer. The overlap charge Y increases from CuCl to CuI, as is expected in this model. The measured elastic constants (Table II) are rather well reproduced. Since the splitting of the total electronic polarizability into contributions from the individual ions is to some extent arbitrary, we compare here only the calculated polarizability per unit cell with the values obtained by the Clausius-Mossotti relation from the high-frequency dielectric constant ϵ_∞, although the application of this relation in covalent crystals may be questioned. In view of these uncertainties the agreement for all three compounds is quite satisfactory, although the small discrepancies in α_∞ have large effects on ϵ_∞.

Similar trends are found for the valence-overlap-shell model in which the $k_{r_2\theta}$ terms are replaced by $k_{\theta\theta}$ terms.

TABLE I. Parameters of the different shell models (λ and all k's in units of e^2/v_a; Z and Y in units of the proton charge e).

	CuCl		CuBr		CuI	
	VOSM	VSM	VOSM	VSM	VOSM	VSM
λ	19.270 72	15.380 29	21.475 80	19.119 33	25.545 2	23.031 45
$k_{r_1\theta}$	3.536 79	1.842 26	4.075 65	2.692 55	5.588 84	3.024 44
$k'_{r_1\theta}$	−0.644 67	0.232 97	−0.554 37	−0.145 73	−1.446 74	0.428 07
$k_{r_2\theta}$	−0.538 87	0.149 03	−0.395 29	0.331 35	−1.908 77	−0.095 34
$k'_{r_2\theta}$	−0.241 29	−0.405 16	−0.138 01	−0.340 72	1.389 28	0.176 30
Z	1.318 91	0.881 30	1.212 64	0.735 26	1.278 71	0.876 02
Y_1	3.201 65	0.476 33	3.636 48	−0.287 44	3.876 91	−0.702 67
Y_2	−1.266 84	−3.649 64	−1.018 06	−2.223 70	−0.732 24	−4.149 07
k_1	47.508	26.349	80.436	31.101	105.510	67.935
k_2	53.311	205.635	59.583	94.714	94.158	196.910
χ	0.07	0.05	0.06	0.05	0.08	0.08
	DSM1	DSM2	DSM1	DSM2	DSM1	DSM2
λ	15.602 55	15.861 50	18.289 15	18.991 75	22.893 65	22.219 20
$k_{r_1\theta}$	2.084 95	2.183 42	2.234 51	2.616 35	2.799 51	2.952 09
$k'_{r_2\theta}$	−0.174 09	−0.290 46	−0.131 70	−0.280 86		
Z	0.868 47	0.930 42	0.895 72	0.994 60	0.945 92	0.957 37
Y_1	0.671 74	0.304 21	0.543 07	0.334 55	−0.884 17	−0.866 55
Y'_1	−1.309 36	−0.191 75	−1.277 85	−0.747 70		
Y_2	−1.127 62	−2.699 55	−1.502 94	−2.681 46	−2.067 65	−2.380 00
Y'_2	$=Y_2$	−0.415 41	$=Y_2$	−0.531 22	$=Y_2$	−1.881 40
$k_1=k'_1$	34.329	32.869	36.124	40.188	90.786	89.394
$k_2=k'_2$	82.860	82.743	91.952	78.529	79.533	81.133
χ	0.06	0.06	0.05	0.04	0.08	0.08

The fits with this model are slightly better in the case of CuI only.

We have also studied valence-shell models for all three compounds. The general trends in the short-range coupling parameters are similar to those of the valence-overlap-shell model. In the simple-shell model the ionic charges assume reasonable values smaller than 1. For CuCl only a second "overlap" minimum is found which has a small positive charge on the Cu^+ shell, whereas for CuBr and CuI only minima with negative shell charges of the Cu^+ ions are found. For CuBr even a second minimum not shown in Table I is found. Replacing again in the short-range potential $k_{r_2\theta}$ by $k_{\theta\theta}$ we find corresponding minima with slightly larger least-squares deviations. In this case the shell charge of the Cu^+ ion in CuCl is negative.

The models discussed so far contain only the dipolar terms, which arise from the displacement induced deformations of the electronic charge density. The higher-order multipole terms of the charge-density deformation are adsorbed in the valence-force-field coupling constants. To get a better understanding of the effects of the higher-order multipole contributions, we have also studied the double-shell models described in the preceding section. It turns out that very good fits of the phonon dispersion curves can be obtained with these double-shell models, which do not involve more parameters than the simple shell model.

In a first approximation we assume equal charges for both shells of the halogen ions (DSM1). This means that the electrical polarization part can still be treated in an effective dipolar approximation. It should, however, be mentioned that the deformation part goes beyond the dipolar approximation and includes also higher-order multipole terms. On the copper site, we allow for two different shell charges. It turns out that in this model some of the valence-force-field constants assume very small values and can be neglected. This has to be attributed to the fact that the double-shell model describes in a more natural way the short-range deformation interactions due to higher-order multipole deformation of the charge density. In this model (DSM1) nine adjustable parameters are needed to reproduce the measured dispersion curves for CuCl and CuBr. For CuI even the second shell at the Cu^+ site can be dropped out completely. This results in a seven-parameter model.

The general trends in the short-range parameters for the three compounds are similar to those discussed earlier. The ionic charge is slightly smaller than 1 for all compounds. The charges of the first shell of the Cu^+ ion are

TABLE II. Macroscopic quantities calculated with different models. Elastic constants c_{ij} in units of 10^{11} dyn/cm^2; electronic polarizabilities α_∞ in units of v_a.

	VOSM	VSM	DSM1	DSM2	Experimental
			CuCl		
c_{11}	5.800	5.210	5.450	5.336	5.53[a]
c_{12}	4.339	4.089	3.983	4.113	4.58[a]
c_{44}^D	1.477	1.883	1.640	1.803	1.68[a]
c_{44}^E	1.474	1.390	1.517	1.448	1.305[a]
α_∞	0.169	0.063	0.088	0.082	0.111[b]
ϵ_0	13.42	3.35	4.54	4.13	5.95[c]
ϵ_∞	8.20	2.07	2.76	2.55	3.61[d]
			CuBr		
c_{11}	5.733	5.708	5.139	5.319	4.58[e]
c_{12}	4.202	4.371	3.823	3.965	3.58[e]
c_{44}^D	1.714	1.561	1.470	1.639	1.49[e]
c_{44}^E	1.515	1.325	1.437	1.453	1.39[e]
α_∞	0.141	0.053	0.096	0.096	0.133[b]
ϵ_0	8.30	2.85	4.64	4.62	6.6[f]
ϵ_∞	5.30	1.86	3.02	3.02	3.71[f]
			CuI		
c_{11}	5.517	5.550	5.207	5.282	4.51[e]
c_{12}	3.900	3.749	3.414	3.447	3.07[e]
c_{44}^D	1.896	1.625	1.517	1.581	1.85[e]
c_{44}^E	1.642	1.590	1.515	1.581	1.82[e]
α_∞	0.120	0.093	0.103	0.106	0.134[b]
ϵ_0	6.53	4.87	5.61	5.60	6.5[f]
ϵ_∞	4.04	2.92	3.27	3.40	4.84[f]

[a]Reference 62. Extrapolated at 5 K.
[b]Calculated from ϵ_∞.
[c]Reference 63.
[d]Reference 25.
[e]Reference 64. At room temperature.
[f]Reference 65 and references therein.

positive in CuCl and CuBr and can be interpreted as overlap charges. In CuI the only shell leftover is coupled to first neighbors and assumes negative values for the charge. The simultaneous vanishing of the effective Cu-Cu short-range interaction represented by $k'_{r_2\theta}$ indicates that the direct Cu-Cu correlations are blocked by the extended wave functions of the I ions. This may be favoring the fast ionic conductivity of the Cu^+ ions in CuI. This version of the double-shell model (DSM1) gives the best results for the dielectric constants. If we replace the short-range force constant $k_{r_2\theta}$ by $k_{\theta\theta}$ we get less satisfactory fits. Moreover, none of the parameters turns out to be small.

Finally, we have relaxed the condition of equal charges for the halogen shells (DSM2). This results in a slight improvement of the fits. Relaxing the condition of equal charges influences substantially the angular part of the valence force field.

We found that this model is the best to describe the pressure-dependent properties of the copper halides as will be discussed in the third paper of this series.

All models discussed here give very satisfactory descriptions of the measured phonon dispersion curves with ten to seven parameters. The main difference between the various models is the way in which the displacement-induced deformation contributions are separated from the short-range overlap parts.

In Figs. 2–4 the phonon dispersion curves calculated with the VOSM (solid lines) and the DSM1 (dashed lines) are compared with the results of the inelastic neutron scattering measurements. It can be seen that both models reproduce the measured data within the limits of the experimental errors, thus providing a good basis for the calculation of solid-state properties which involve phonons and phonon densities.

The one-phonon densities of states (Fig. 5) have been calculated with the VOSM by sampling the frequencies calculated on a fine mesh in the irreducible part of the Brillouin zone. The spectrum of CuCl has a three-band structure. The lowest band arises essentially from the low-frequency transverse acoustic branches, which are very flat and thus give rise to a narrow band with a high density of states. The higher-frequency longitudinal branches are less flat and contribute to the broad second band, which is separated by an energy gap from a relatively wide optic band. CuBr shows a similar spectrum. The TA and the LA bands are broader. Optic and acoustic bands are again separated by a gap. The optic bands are narrower than those of CuCl, since the optic branches of CuBr show less dispersion. The spectrum of CuI shows two broad structures arising from the TA and LA branches. It is interesting to note that the gap between the highest acoustic and the lowest optic band has shrunk to one channel and that the TO and LO bands are now separated by a relatively wide gap. The LO and TO branches are flat and show little dispersion. This gives rise to narrow bands with high densities of states.

A final remark concerns the lattice dynamics of AgI, which is also a borderline case between an ionic and a covalent crystal close to the tetrahedral-octahedral phase transition just as is CuI. At atmospheric pressure the wurtzite structure (β phase) coexists with the cubic face-centered zinc-blende structure (γ phase). AgI undergoes

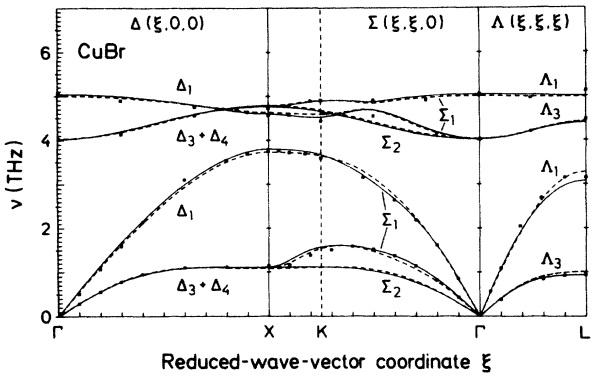

FIG. 3. Phonon dispersion curves of CuBr at 77 K. The solid and dashed curves are calculated using the VOSM and the DSM1, respectively. The symbols represent the measured data of Hoshino *et al.* (Ref. 34).

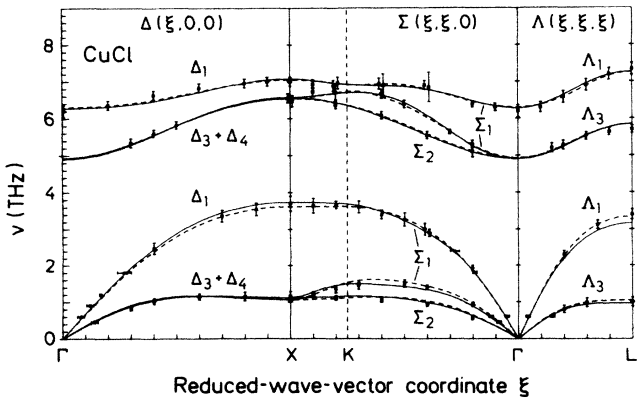

FIG. 2. Phonon dispersion curves of CuCl at 4.2 K. The solid and dashed curves are calculated using the VOSM and the DSM1, respectively. The symbols represent the measured data of Prevot *et al.* (Ref. 33).

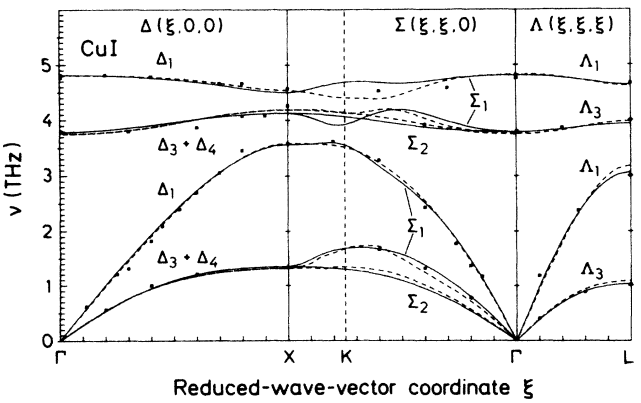

FIG. 4. Phonon dispersion curves of CuI at room temperature. The solid and dashed curves are calculated using the VOSM and the DSM1, respectively. The symbols represent the measured data of Hennion *et al.* (Ref. 32).

at 420 K a phase transition[60] into the cubic α phase in which the Ag^+ ion occupies one of the 12 equivalent lattice sites. α-AgI is a classical superionic conductor. The phonon dispersion curves of β-AgI have been studied by inelastic neutron scattering measurements at 160 K,[61] but up to now no measurements of the phonon dispersion curves in the metastable γ phase exist since γ-AgI occurs only in powdered form.

Since Ag^+ has an electronic configuration similar to Cu^+ it can be expected that the interionic coupling constants of both compounds are very similar and that the difference in the phonon dispersion curves of the two compounds is essentially due to the differences in the masses and in the lattice constants. We have therefore calculated the dispersion curves of γ-AgI assuming the same coupling constants as for CuI. The results obtained with the DSM2 are given in Fig. 6 by the solid lines. Bührer *et al.*[61] calculated the phonon dispersion curves of γ-AgI (dashed lines) using valence force constants fitted to the experimental data of the β phase. They compare their results with scaled experimental data of CuBr (open squares).

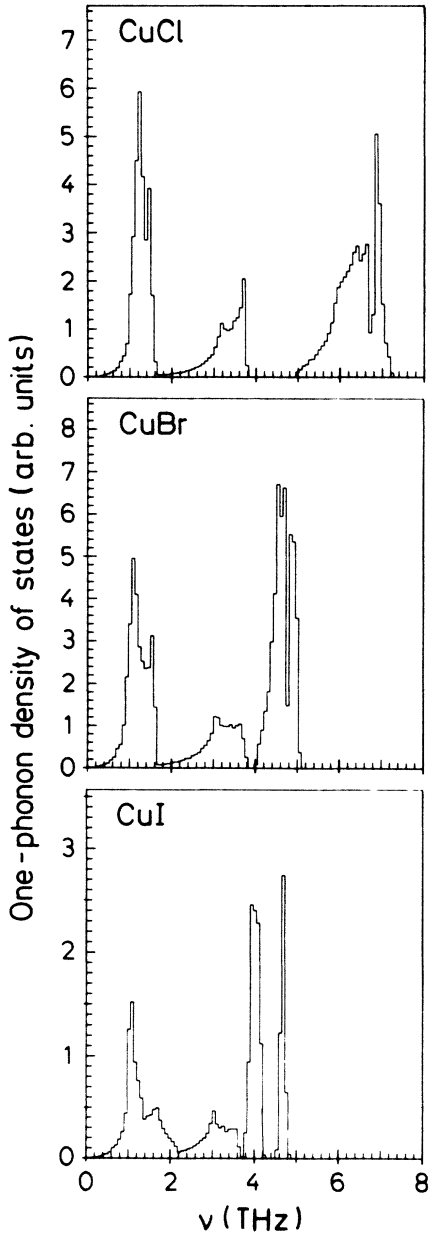

FIG. 5. One-phonon densities of states of CuCl, CuBr, and CuI calculated with the VOSM. The model parameters are fitted to the dispersion curves of CuCl, CuBr, and CuI measured at 4.2 K, 77 K, and room temperature, respectively.

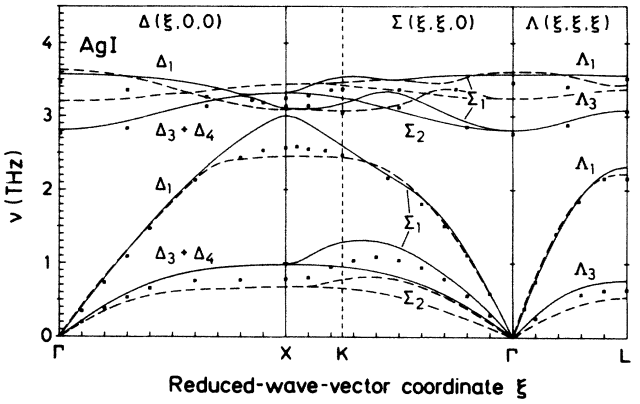

FIG. 6. Phonon dispersion curves of γ-AgI. The solid curves are calculated with the DSM2 of CuI taking into account the masses and lattice constant of AgI. The dashed curves are calculated by Bührer *et al.* (Ref. 61) using a VSM fitted to the data of β-AgI. The symbols are the CuBr data scaled by the homology criterion of interatomic forces.

The overall agreement with the optical branches is much better in our calculations, whereas we obtain higher frequencies for the acoustical branches in the regions close to the zone boundaries. In these regions the scaling of the CuBr may be questioned in view of the systematic trends of zone-edge acoustic phonons in CuCl, CuBr, and CuI towards higher frequencies. The deviations between the scaled CuBr data and the results of Bührer *et al.*[61] may be attributed to the fact that part of the short-range Coulomb interaction absorbed in valence force field cannot be transferred properly from one structure to the other. With respect to our results the question remains to what extent the Ag-I short-range interactions can be approximated by the Cu-I interactions. On the other hand, it should be mentioned that the slight enhancement of the Ag^+ polarizability (in units of v_a) will only have minor effects on the dispersion curves, since the polarizability per unit cell is essentially determined by the I^- contribution.

V. SUMMARY AND CONCLUSIONS

We have analyzed the phonon dispersion curves of CuCl, CuBr, and CuI using different versions of valence-shell models. The measured phonon dispersion curves are very well reproduced by three different models: a valence-overlap-shell model, a simple-shell model, and a double-shell model. Although there are some differences in the least-squares deviations which are obtained with the

different models in a least-squares-fitting procedure, these deviations are so small for all models that each of them reproduces the measured dispersion curves with sufficient accuracy. The main difference between the various models which have been investigated here lies in the separation of short-range overlap forces and displacement-induced deformability contributions. With a double-shell model the dispersion curves can be described with only three short-range parameters which are derived from a valence-force-field potential. The results of the present study will serve as a basis for the investigation of the anomalous line shapes of the TO(Γ) phonons which have been observed in these compounds. The results will be presented in the second paper of this series. The pressure effects on the phonon dispersion curves and the phonon line shapes will be treated in a third paper.

ACKNOWLEDGMENT

We would like to thank K. Kunc for providing us with some of the computer programs.

---

*Permanent address: Physics Department, University of Thessaloniki, Thessaloniki, Greece.

[1]J. C. Phillips, Rev. Mod. Phys. **42**, 317 (1970).
[2]S. Hoshino, J. Phys. Soc. Jpn. **7**, 560 (1952).
[3]E. Rappaport and C. W. F. T. Pistorius, Phys. Rev. **172**, 838 (1968).
[4]O. Brafman, M. Cardona, and Z. Vardeny, Phys. Rev. B **15**, 1081 (1977).
[5]S. Miyake, S. Hoshino, and T. Takenaka, J. Phys. Soc. Jpn. **7**, 19 (1952).
[6]S. Miyake and S. Hoshino, Rev. Mod. Phys. **30**, 172 (1958).
[7]V. Valdova and J. Jecny, Phys. Status Solidi A **45**, 269 (1978).
[8]J. M. Tranquada and R. Ingalls, Phys. Rev. B **28**, 3520 (1983).
[9]M. Sakata, S. Hoshino, and J. Harada, Acta Crystallogr. Sect. A **30**, 655 (1974).
[10]J. Harada, H. Suzuki, and S. Hoshino, J. Phys. Soc. Jpn. **41**, 1707 (1976).
[11]K. D. Becker, G. W. Herzog, D. Kanne, H. Richtering, and E. Stadler, Ber. Bunsenges. Phys. Chem. **75**, 527 (1970).
[12]C. Clemen and K. K. Funke, Ber. Bunsenges. Phys. Chem. **79**, 1119 (1975).
[13]M. Krauzman, in *Light Scattering Spectra of Solids*, edited by G. B. Wright (Springer-Verlag, Berlin, 1969), p. 109.
[14]M. A. Nusimovici and A. Meskini, Phys. Status Solidi B **52**, K62 (1972).
[15]T. Fukumoto, K. Tabuchi, S. Nakashima, and A. Mitsuishi, J. Phys. Soc. Jpn. **35**, 622 (1973).
[16]B. Prevot and M. Sieskind, Phys. Status Solidi B **59**, 133 (1973).
[17]J. E. Potts, R. C. Hanson, C. T. Walker, and C. Schwab, Phys. Rev. B **9**, 2711 (1974).
[18]I. P. Kaminow and E. H. Turner, Phys. Rev. B **5**, 1564 (1972).
[19]M. L. Shand, L. Y. Ching, and E. Burstein, Solid State Commun. **15**, 1209 (1974).
[20]M. Krauzman, R. M. Pick, H. Poulet, G. Hamel, and B. Prevot, Phys. Rev. Lett. **33**, 528 (1974).
[21]T. Fukumoto, S. Nakashima, K. Tabuchi, and A. Mitsuishi, Phys. Status Solidi B **73**, 341 (1976).
[22]H. D. Hochheimer, M. L. Shand, J. E. Potts, R. C. Hanson, and C. T. Walker, Phys. Rev. B **14**, 4630 (1976).
[23]A. Blacha, Ph.D. thesis, University of Stuttgart, 1985 (unpublished).
[24]A. Blacha, G. Kourouklis, and M. Cardona (unpublished).
[25]Z. Vardeny and O. Brafman, Phys. Rev. B **19**, 3276 (1979).
[26]B. Hennion, B. Prevot, M. Krauzman, R. M. Pick, and B. Dorner, J. Phys. C **12**, 1609 (1979).
[27]G. Burns, I. H. Dacol, M. W. Shafer, and R. Albey, Solid State Commun. **24**, 753 (1974).
[28]G. Kanellis, W. Kress, and H. Bilz, Phys. Rev. B **33-II**, 8733 (1986).
[29]G. Kanellis, W. Kress, and H. Bilz (unpublished).
[30]C. Carabatos, B. Hennion, K. Kunc, F. Moussa, and C. Schwab, Phys. Rev. Lett. **26**, 770 (1971).
[31]B. Prevot, C. Carabatos, C. Schwab, B. Hennion, and F. Moussa, Solid State Commun. **13**, 1725 (1973).
[32]B. Hennion, F. Moussa, B. Prevot, C. Carabatos, and C. Schwab, Phys. Rev. Lett. **28**, 964 (1972).
[33]B. Prevot, B. Hennion, and B. Dorner, J. Phys. C **10**, 3999 (1977).
[34]S. Hoshino, Y. Fujii, J. Harada, and J. S. Axe, J. Phys. Soc. Jpn. **41**, 965 (1976).
[35]R. Banerjee and Y. P. Varshni, Solid State Commun. **9**, 2115 (1971).
[36]B. P. Pandey, Phys. Lett. **50A**, 215 (1974).
[37]Z. Vardeny, G. Gilat, and A. Pasternack, Phys. Rev. B **11**, 5175 (1975).
[38]M. S. Kushwaha, Can. J. Phys. **60**, 1589 (1982).
[39]B. P. Pandey and B. Dayal, Solid State Commun. **15**, 1667 (1974).
[40]M. V. Haxton, Phys. Status Solidi B **86**, 661 (1978).
[41]S. Chatterjee, S. Gosh, and A. N. Basu, Phys. Rev. B **28**, 3534 (1983).
[42]P. Plumelle, D. N. Talwar, M. Vandevyver, K. Kunc, and M. Zigone, Phys. Rev. B **20**, 4199 (1979).
[43]M. Vandevyver and P. Plumelle, Phys. Rev. B **17**, 675 (1978); J. Phys. Chem. Solids **38**, 765 (1977); Phys. Status Solidi B **73**, 271 (1976).
[44]D. N. Talwar, M. Vandevyver, K. Kunc, and M. Zigone, Phys. Rev. B **24**, 741 (1981).
[45]K. Kunc and H. Bilz, Solid State Commun. **19**, 1027 (1976).
[46]K. Kunc and H. Bilz, in *Proceedings of the Conference on Neutron Scattering, Report No. CONF-760601-P1, Gatlinburg, Tennessee, 1976*, edited by R. M. Moon (National Technical Information Service, U.S. Department of Commerce, Springfield, Virginia, 1976), Vol. 1, p. 195.
[47]B. C. Dick and A. W. Overhauser, Phys. Rev. **112**, 90 (1958).
[48]W. Cochran, Proc. R. Soc. London, Ser. A **253**, 260 (1959).
[49]L. A. Feldkamp, D. K. Steinman, N. Vagelatos, J. S. King, and G. Venkataraman, J. Phys. Chem. Solids **32**, 1573 (1971).
[50]K. Kunc and O. H. Nielsen, Comput. Phys. Commun. **17**, 413 (1979).
[51]R. Tubino, L. Piseri, and G. Zerbi, J. Chem. Phys. **56**, 1022

(1972).
[52]W. Solbrig, Phys. Chem. Solids **32**, 1761 (1971).
[53]R. Haberkorn, M. Buchanan, and H. Bilz, Solid State Commun. **12**, 681 (1973).
[54]M. Buchanan, R. Haberkorn, and H. Bilz, J. Phys. C **7**, 439 (1974).
[55]R. Migoni, Ph.D. thesis, University of Stuttgart, 1976 (unpublished).
[56]R. Migoni, H. Bilz, and D. Bäuerle, Phys. Rev. Lett. **37**, 1155 (1976).
[57]R. A. Cowley, Proc. R. Soc. London, Ser. A **268**, 109 (1962).
[58]H. Bilz, D. Strauch, and R. K. Wehner, *Handbuch der Physik-Encyclopedia of Physics,* edited by S. Flügge (Springer-Verlag, Berlin, 1984), Vol. XXVI/2d.
[59]W. Weber, Phys. Rev. B **8**, 5082 (1973).
[60]W. Bührer and W. Hälg, Helv. Phys. Acta **47**, 27 (1974).
[61]W. Bührer, R. M. Nicklow, and P. Brüesch, Phys. Rev. B **17**, 3362 (1978).
[62]R. C. Hanson, K. Helliwell, and C. Schwab, Phys. Rev. B **9**, 2649 (1974).
[63]J. E. Potts, R. C. Hanson, C. T. Walker, and C. Schwab, Phys. Rev. B **9**, 2711 (1974).
[64]R. C. Hanson, J. R. Hallberg, and C. Schwab, Appl. Phys. Lett. **21**, 490 (1972).
[65]J. E. Potts, R. C. Hanson, C. T. Walker, and C. Schwab, Solid State Commun. **13**, 389 (1973).

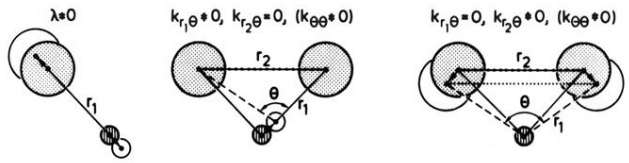

FIG. 1. Schematic representation of the valence-force-field coupling constants.